ISSN 1063-7834, Physics of the Solid State, 2015, Vol. 57, No. 3, pp. 491–498. © Pleiades Publishing, Ltd., 2015.
Original Russian Text © I.N. Safonov, S.V. Misyul', M.S. Molokeev, M.P. Ivliev, 2015, published in Fizika Tverdogo Tela, 2015, Vol. 57, No. 3, pp. 480–486.

**PROCEEDINGS OF THE XX ALL-RUSSIA CONFERENCE ON PHYSICS OF FERROELECTRICS (VKS-XX)**
**(Krasnoyarsk, Russia, August 18–22, 2014)**

# Structural Transformations and Phenomenological Description of the Formation of Phase States in Elpasolites $Cs_2RbDyF_6$ and $Rb_2KB'F_6$ ($B'$ = Ho, Dy, Tb)

**I. N. Safonov[a, *], S. V. Misyul'[a], M. S. Molokeev[b], and M. P. Ivliev[c]**

[a] *Siberian Federal University, Svobodnyi pr. 79, Krasnoyarsk, 660041 Russia*
[*] *e-mail: isafonov@sfu-kras.ru*
[b] *Kirensky Institute of Physics, Siberian Branch of the Russian Academy of Sciences, Akademgorodok 50–38, Krasnoyarsk, 660036 Russia*
[c] *Research Institute of Physics, Southern Federal University, pr. Stachki 194, Rostov-on-Don, 344090 Russia*

**Abstract**—The structures of the cubic and monoclinic phases of an $Rb_2KHoF_6$ crystal from a series of elpasolites $Rb_2KB'F_6$ ($B'$ = Ho, Dy, Tb), which undergoes a trigger phase transition, have been investigated using X-ray powder diffraction. The critical and noncritical displacements of atoms in the $Rb_2KHoF_6$ structure have been determined from the group-theoretical analysis of the complete condensate of order parameters. It has been reliably established that a change in the symmetry due to the phase transition in this crystal can be represented in the form $Fm\bar{3}m \xrightarrow[(\varphi, \varphi, \psi)]{11-9(\Gamma_4^+) \oplus 10-3(X_3^+)} P12_1/n1$. A phenomenological analysis of the conditions responsible for the formation of phase states upon the phase transitions in elpasolites $Cs_2RbDyF_6$ and $Rb_2KB'F_6$ ($B'$ = Ho, Dy, Tb) has been carried out. Taking into account the structural data and using the phenomenological theory, it has been found that the main factor determining the formation of phase states in these and related crystals is the instability of the elpasolite structure with respect to rotational distortions of two types. It has been shown that an important role in the formation of a sequence of structural transformations in these crystals is played by the interaction of rotational order parameters and displacements of the cation from the center of a cuboctahedral hole.

**DOI:** 10.1134/S1063783415030282

## 1. INTRODUCTION

Halide compounds of the elpasolite family $A_2BB'X_6$ ($A$ = Cs, Rb; $B$ = Na, K, Rb; $B'$ = Ga, Sc, In, Ho, Dy, Tb, Nd, Pr, Bi; $X$ = F, Cl) belong to a large group of crystals whose lattice can be represented as a three-dimensional framework formed by different-size octahedral groups $B'X_6$ and $BX_6$, which alternate in three directions of the [001] type. The adjacent octahedra $B'X_6$ and $BX_6$ are joined together through the common vertex, and the $A$ cations are located in inter-octahedral (cuboctahedral) holes [1, 2]. In the initial high-temperature phase $G_0$, the crystals have cubic symmetry (space group $O_h^5 - Fm\bar{3}m$, $Z = 4$). As the temperature decreases, the crystals undergo ferroelastic phase transitions. The majority of phase transitions in these compounds are caused by an instability of the framework with respect to atomic displacements, which can be interpreted as rotations of φ- and ψ-type octahedra [1, 2].

The group-theoretical analysis of lattice vibrations and the analysis of the elpasolite structure [3–5] demonstrate that the order parameters corresponding to librational vibrations of the octahedra transform according to the irreducible representations $11-9(\Gamma_4^+)$ and $10-3(X_3^+)$ of the center (the Γ point) and the boundary (the $X$ point) of the Brillouin zone of the group $O_h^5 - Fm\bar{3}m$, respectively (designations of the irreducible representations correspond to [6, 7]). Irreducible and reducible representations that induce changes of the symmetry are commonly referred to as critical or primary representations.

A set of reducible representations, both critical and noncritical, which appear during phase transitions, forms a complete condensate of reducible representations [8]. According to [9], in crystals with the initial phase $O_h^5 - Fm\bar{3}m$, critical distortions are accompanied by secondary (noncritical) effects, such as distortions of octahedral groups, displacements of atoms located in inter-octahedral holes, etc. Numerical values of critical and noncritical distortions and reducible representations are determined from experimental data.

**Table 1.** Main thermodynamic characteristics of the phase transitions in elpasolite $Cs_2RbDyF_6$ and $Rb_2KB'F_6$ ($B'$ = Ho, Dy, Tb) [10–14]

| Crystal | $G_i$ | $Z$ | System of octahedral rotation | $T_i$, K | $\delta T_i$, K | $\Delta S/R$ |
|---|---|---|---|---|---|---|
| $Cs_2RbDyF_6$ | $C_{4h}^5$–$I1\ 14/m$ | 2 | φ00 | 251 | 0 | 0.20 |
| | $C_{2h}^3$–$I12/m1$ | 2 | φφ0 | 205 | 0.10 | 0.47 |
| | $C_{2h}^5$–$P12_1/n1$ | 2 | φφψ | 196 | 0 | |
| $Rb_2KHoF_6$ | $C_{2h}^5$–$P12_1/n1$ | 2 | φφψ | 400 | 1.27 | 0.65 |
| $Rb_2KDyF_6$ | $C_{2h}^5$–$P12_1/n1$ | 2 | φφψ | 390 | | 0.52 |
| $Rb_2KTbF_6$ | $C_{2h}^5$–$P12_1/n1$ | 2 | φφψ | 412 | | 0.67 |

Designations: $G_i$ is the space group of the dissymmetric phase, $Z$ is the number of formula units in the Bravais cell, $T_i$ is the phase transition temperature, $\delta T_i$ is the hysteresis of the phase transition temperature, $\Delta S/R$ is the entropy change due to the phase transition, and $R$ is the gas constant.

Sequences of phase transitions in crystals $Cs_2RbDyF_6$ and $Rb_2KB'F_6$ ($B'$ = Ho, Dy, Tb) were investigated in [10–14]. In [10, 11], it was found that, with a decrease in the temperature, the $Cs_2RbDyF_6$ crystal undergoes three phase transitions (Table 1). According to experimental data [11, 12], there is a sequence of critical distortions, namely, (000) ⟶ (φ00) ⟶ (φφ0) ⟶ (φφψ), which is accompanied by changes of the symmetry (see Table 1). In contrast to the $Cs_2RbDyF_6$ crystal, the $Rb_2KB'F_6$ ($B'$ = Ho, Dy, Tb) crystals [13, 14] undergo only one phase transition in which the symmetry is reduced immediately to the monoclinic symmetry with multiplication of the crystal cell and the distortions are described by the scheme (000) ⟶ (φφψ) (Table 1). However, the presented scheme of distortions was obtained from indirect data. It should be noted that the crystal-chemical characteristics of the crystals $Cs_2RbDyF_6$ and $Rb_2KB'F_6$ ($B'$ = Ho, Dy, Tb) are very close to each other, even though sets of dissymmetric phases in them differ significantly. The reason for these differences is not completely understood.

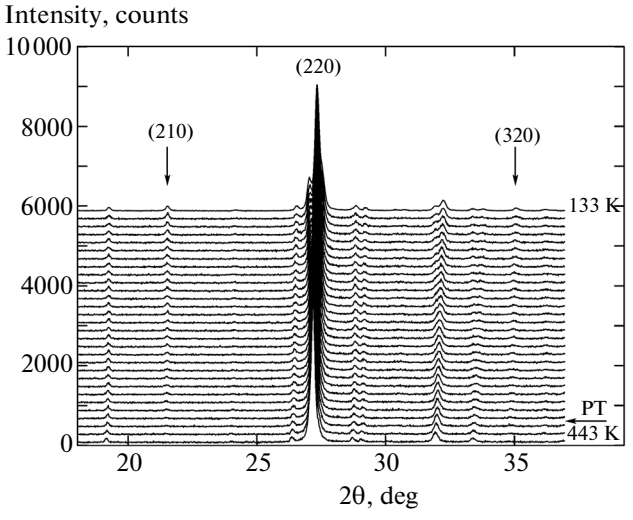


**Fig. 1.** Fragments of X-ray diffraction patterns of the $Rb_2KHoF_6$ crystal (arrows indicate superstructure reflections in the monoclinic phase). The arrow PT shows the phase transition point.

The purpose of this work is as follows: (1) to determine the structures of the cubic and monoclinic phases of the $Rb_2KHoF_6$ crystal; (2) to identify the critical and noncritical distortions and reducible representations in $Rb_2KHoF_6$; (3) to elucidate the conditions for the existence of sequences of orderings in $Rb_2KB'F_6$ ($B'$ = Ho, Dy, Tb) and $Cs_2RbDyF_6$ in the framework of the phenomenological theory; and (4) to analyze factors that determine the formation of particular sets of phase states.

## 2. EXPERIMENTAL TECHNIQUE AND RESULTS

The structures of the phases of the $Rb_2KHoF_6$ crystal were determined from X-ray diffraction experiments for powder samples. The X-ray diffraction patterns of the $Rb_2KHoF_6$ compound were measured using an Anton Paar TTK 450 low-temperature chamber mounted on a Bruker D8-ADVANCE X-ray diffractometer ($CuK_\alpha$ radiation, θ–2θ scan mode, VANTEC linear detector). Liquid nitrogen was used as a coolant. The scan step in the 2θ range was 0.016°, and the exposure time per point was 3 s. In the temperature range from 133 to 463 K, 32 X-ray diffraction patterns were measured in steps of 10 and 20 K in the monoclinic phase $G_1$ and cubic phase $G_0$, respectively.

**Table 2.** Crystallographic data, data collection and refinement parameters of the $Rb_2KHoF_6$ structure for two temperatures of the experiment

| Parameter | $T = 463$ K | $T = 133$ K |
|---|---|---|
| Space group | $O_h^5$–$Fm\bar{3}m$ | $C_{2h}^5$–$P12_1/n1$ |
| $a_i$, Å | $\mathbf{a}_0$, 9.3143(3) | $1/2(\mathbf{a}_0 - \mathbf{b}_0)$, 6.4889(4) |
| $b_i$, Å | $\mathbf{b}_0$, 9.3143(3) | $1/2(\mathbf{a}_0 + \mathbf{b}_0)$, 6.6081(4) |
| $c_i$, Å | $\mathbf{c}_0$, 9.3143(3) | $\mathbf{c}_0$, 9.2271(5) |
| β, deg | 90 | 90.178(4) |
| $Z$ | 4 | 2 |
| $V$, Å$^3$ | 808.07(1) | 395.65(4) |
| 2θ range in the X-ray diffraction pattern, deg | 5–110 | 5–110 |
| Integral Bragg factor $R_B$, % | 2.0 | 0.9 |
| Weighted profile $R$-factor $R_{wp}$, % | 7.4 | 7.4 |

The symmetry and parameters of the $Rb_2KHoF_6$ crystal cells in the cubic and monoclinic phases were determined earlier in [13]. These data were used in our present study. The superstructure reflections (Fig. 1) in the X-ray diffraction patterns of the $Rb_2KHoF_6$ monoclinic phase confirmed the doubling of the primitive cell volume upon the phase transition (Table 2).

The profile and structural parameters were refined with the TOPAS software package [15]. The first stage of the processing of the experimental data included the procedure of fitting of the profile and shape of X-ray diffraction peaks. As a result of this data processing, we obtained the temperature dependences of the parameters of the crystal cell (Fig. 2) and monoclinic angle (Fig. 3). Table 2 presents the main parameters of the data collection and refinement of the structure only for two temperatures, namely, 463 K (cubic phase) and 133 K (monoclinic phase), which are the most distant from the phase transition point. It is for these temperatures that the results of the refinement will be presented below.

The second stage of the data processing included the refinement of the coordinates and thermal parameters of atoms in the $Rb_2KHoF_6$ crystal. The structure of the cubic phase was determined taking into account that all atoms are located in special locations. Therefore, in the cubic phase of the $Rb_2KHoF_6$ crystal, we refined only five parameters: the coordinate $x$ of the fluorine atom and isotropic thermal parameters for all the considered atoms (Table 3).

For the distorted monoclinic phase, the initial coordinates of atoms were taken as the coordinates of these atoms in the cubic phase. After several cycles of

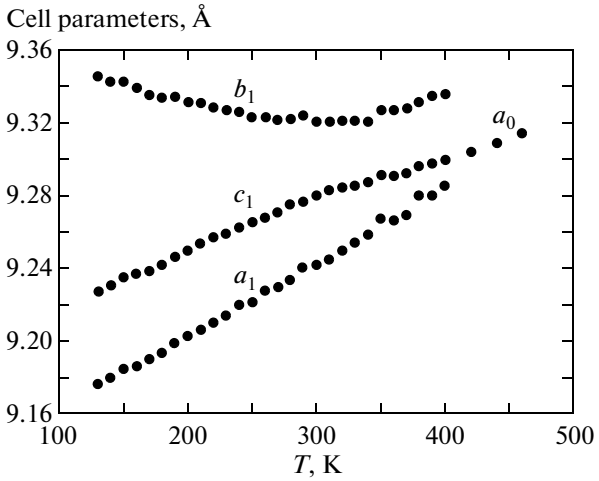


**Fig. 2.** Dependences of the lattice parameters of the $Rb_2KHoF_6$ crystal $a_0$ (cubic phase) and $a_1$, $b_1$, and $c_1$ (monoclinic phase) on the temperature (in the monoclinic phase, the lattice parameters $a_1$ and $b_1$ are increased by a factor of $\sqrt{2}$).

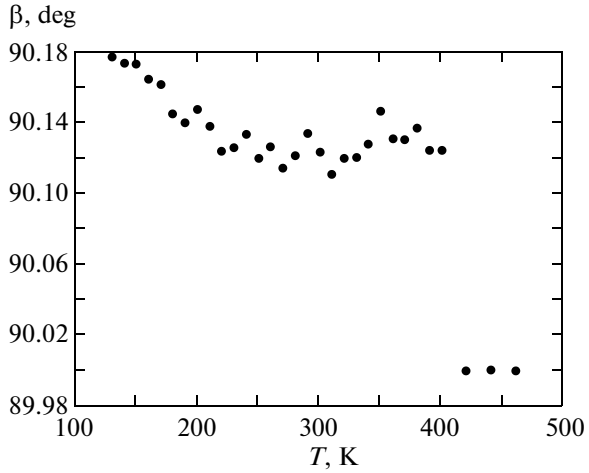


**Fig. 3.** Temperature dependence of the monoclinic cell angle β in the $Rb_2KHoF_6$ crystal.

**Table 3.** Coordinates and isotropic thermal parameters of atoms $B_{iso}$ $Rb_2KHoF_6$ structure at temperatures of 463 and 133 K

| Atom | $x$ | $y$ | $z$ | $B_{iso}$, Å$^2$ |
|---|---|---|---|---|
| | | $T = 463$ K | | |
| Rb | 0.25 | 0.25 | 0.25 | 6.0(1) |
| K | 0 | 0 | 0.5 | 2.5(2) |
| Ho | 0 | 0 | 0 | 3.1(1) |
| F | 0.2344(5) | 0 | 0 | 2.2(2) |
| | | $T = 133$ K | | |
| Rb | 0 | 0.5259(2) | 0.2535(6) | 2.8(1) |
| K | 0 | 0 | 0.5 | 1.2(2) |
| Ho | 0.5 | 0.5 | 0.5 | 1.8(1) |
| F1 | 0.821(3) | 0.264(3) | 0.043(3) | 1.8(2) |
| F2 | 0.219(4) | 0.674(3) | 0.532(3) | 1.9(2) |
| F3 | 0.886(3) | 0.016(3) | 0.763(2) | 1.2(1) |

**Table 4.** Selected bond lengths and angles in the $HoF_6$ octahedron

| | $T = 463$ K | $T = 133$ K |
|---|---|---|
| | Bond length, Å | |
| Ho–F1 | 2.182(5) | 2.13(2) |
| Ho–F2 | | 2.17(2) |
| Ho–F3 | | 2.30(2) |
| K–F1 | 2.474(5) | 2.63(2) |
| K–F2 | | 2.60(2) |
| K–F3 | | 2.55(2) |
| Rb–F1 | 3.223(3) | 2.80(2) |
| Rb–F2 | | 2.82(2) |
| Rb–F3 | | 2.82(2) |
| | Angle, deg | |
| F1–Ho–F2 | 90 | 87.3(8) |
| F1–Ho–F3 | | 88.0(8) |
| F2–Ho–F3 | | 83.6(8) |

the refinement, the discrepancy factors reached a minimum (Table 2).

Table 4 presents the selected bond lengths and angles of the octahedral groups $HoF_6$. The projections of the structures of the cubic and monoclinic phases of the $Rb_2KHoF_6$ crystal are shown in Figs. 4 and 5, respectively. For convenience of the comparison, the structures of the monoclinic phase are projected along the coordinate axes of the initial cubic phase $G_0$. From Tables 3, 4 and Figs. 4, 5, it can be seen that, upon the phase transition, the main changes occur with the coordinates of the fluorine atoms. In general, these displacements can be represented in the form of rotations of rigid octahedra, for example, the $HoF_6$ octahedra. Therefore, according to Figs. 4 and 5, the distortion of the $Rb_2KHoF_6$ crystal can be described by the symbol ($\varphi\varphi\psi$).

A further analysis of the experimental data will be performed based on the group-theoretical analysis of the structural phase transitions in crystals with the space group $Fm\bar{3}m$ [9] and with the use of the ISODISPLACE software [16]. This made it possible to expand the displacements of atoms in the distorted phase in terms of the irreducible representations of the group of the initial phase $Fm\bar{3}m$ and to visualize the obtained result.

So, the displacements of all atoms of the $Rb_2KHoF_6$ structure in the monoclinic phase are divided according to the following irreducible representations: $\Gamma_1^+$, $\Gamma_3^+$, $\Gamma_4^+$, $\Gamma_5^+$, $X_2^+$, $X_3^+$, and $X_5^+$. The critical displacements are the $\varphi$ rotations of the octahedra (representation $\Gamma_4^+$) and the $\psi$ rotations (representation $X_3^+$). After the phase transition, these displacements take the maximum values. All the other displacements, which are transformed according to the irreducible representations $\Gamma_1^+$, $\Gamma_3^+$, $\Gamma_5^+$, $X_2^+$, and $X_5^+$, do not determine the symmetry of the distorted phase and are noncritical.

The distortion of the $HoF_6$ octahedra involves displacements of fluorine atoms that transform according to the irreducible representations $\Gamma_3^+$, $\Gamma_5^+$, $X_2^+$, and $X_5^+$, which have no significant effect on the shape of the octahedra (Tables 3, 4). The totally symmetric displacement $\Gamma_1^+$ causes only a homogeneous deformation of the octahedra. Among all the noncritical displacements, we note displacements of the Rb atom along the face diagonal of the unit cell in the initial phase (irreducible representation $X_5^+$). In the monoclinic phase at 133 K, these displacements are equal to 0.3 Å and comparable with the critical displacements of the fluorine atoms. Thus, although the displacements of Rb atoms are noncritical at temperatures far from the phase transition temperatures, they become significant.

Let us compare the displacements of atoms in the lowest-symmetry monoclinic phase of the $Cs_2RbDyF_6$ crystal [12] with the corresponding displacements in the $Rb_2KHoF_6$ monoclinic phase. The complete condensates of reducible representations for two crystals in the corresponding monoclinic phases coincide with each other. Unlike the displacements of rubidium atoms in $Rb_2KHoF_6$, the displacements of Cs atoms in $Cs_2RbDyF_6$ are very small even in the lowest-symmetry phase (0.05 Å against 0.3 Å) and occur in planes

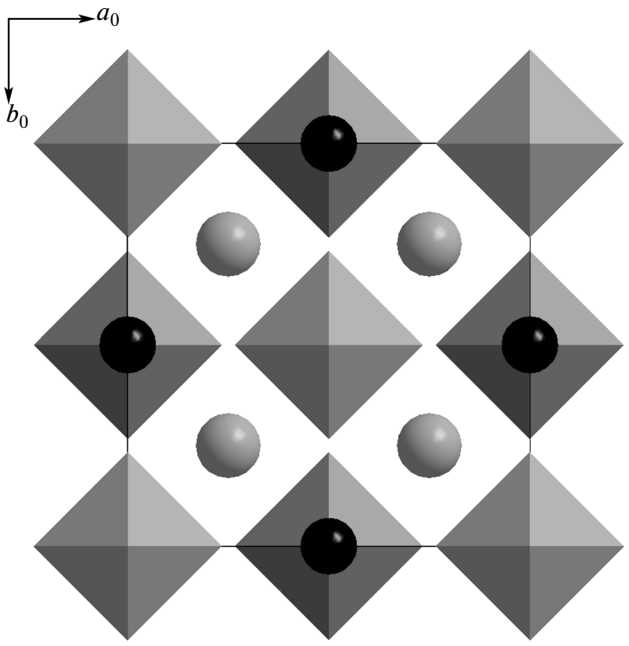


**Fig. 4.** Projection of the $Rb_2KHoF_6$ cubic cell along the fourfold axis at 463 K. Only the $HoF_6$ octahedra are shown. The octahedra are formed by six fluorine atoms located at the vertices. The Ho atoms are located at the center of the octahedra. Black and gray circles are potassium and rubidium atoms, respectively.

with the [001] indices almost along the face diagonal of the cubic unit cell (irreducible representation $X_5^+$). It should be noted that the distortions of the $HoF_6$ octahedral group in $Rb_2KHoF_6$ are not so large as those of the $DyF_6$ groups in $Cs_2RbDyF_6$. At a temperature of 130 K, the angles of rotation of the $DyF_6$ octahedra in $Cs_2RbDyF_6$ take the following values: $\varphi \approx 8°$ and $\psi \approx 5°$. In $Rb_2KHoF_6$ at 133 K, the angles of rotation are $\varphi \approx 12°$ and $\psi \approx 10°$.

Thus, the phase transition in the $Rb_2KHoF_6$ crystal is a displacement-type transition, and the change of the symmetry in the distorted phase can be described by rotations of the $HoF_6$ octahedra.

## 3. FORMATION OF PHASE STATES (PHENOMENOLOGICAL THEORY)

The formation of the phase states (000) $\longrightarrow$ ($\varphi$00) $\longrightarrow$ ($\varphi\varphi$0) $\longrightarrow$ ($\varphi\varphi\psi$) (sequence 1) for $Cs_2RbDyF_6$ and (000) $\longrightarrow$ ($\varphi\varphi\psi$) (sequence 2) for $Rb_2KB'F_6$ ($B'$ = Ho, Dy, Tb), where, as noted above, $\varphi \in \Gamma_4^+$ and $\psi \in X_3^+$ are the critical reducible representations, is analyzed based on the phenomenological theory [17]. A similar analysis was performed for rotational phase transitions in perovskites [18, 19] and for some phase transitions in elpasolites [4].

A simple thermodynamic potential describing the above sequences has the form

$$\Phi(\psi, \varphi) = \Phi_X + \Phi_\Gamma + \Phi_{\Gamma X},$$

where

$$\Phi_\Gamma = \alpha_{1\Gamma}G_{1\Gamma} + \alpha_{2\Gamma}G_{1\Gamma}^2 + \beta_{1\Gamma}G_{2\Gamma} + \sigma_\Gamma G_{1\Gamma}G_{2\Gamma} + \omega_\Gamma G_{3\Gamma} + \ldots,$$

$$\Phi_X = \alpha_{1X}G_{1X} + \alpha_{2X}G_{1X}^2 + \beta_{1X}G_{2X} + \ldots,$$

$$G_{1\Gamma} = \sum_{i=1}^{3}\varphi_i^2, \quad G_{2\Gamma} = \sum_{i=1}^{2}\sum_{j=2(i<j)}^{3}\varphi_i^2\varphi_j^2,$$

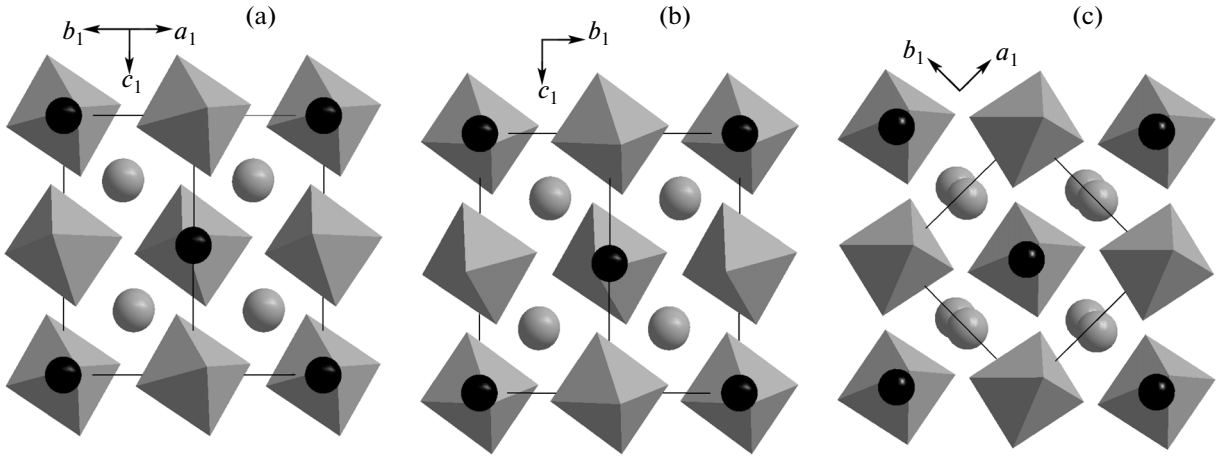


**Fig. 5.** Projections of the initial phase of the $Rb_2KHoF_6$ monoclinic cell along the fourfold axes at 133 K: (a, b) $\varphi$ rotation and (c) $\psi$ rotation. The notation is the same as in Fig. 4.

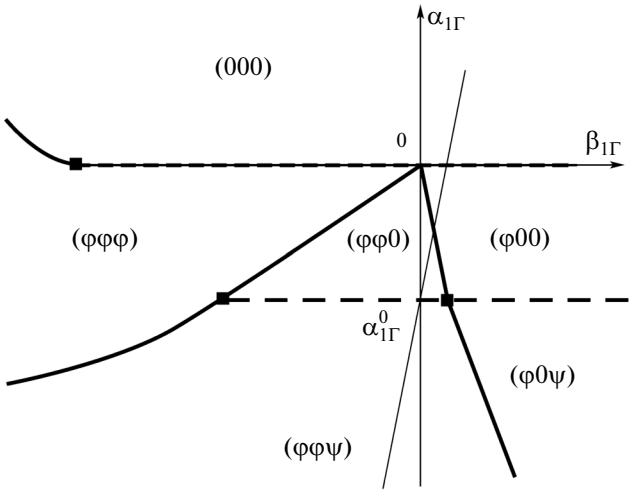


**Fig. 6.** Diagram of phase states described by the thermodynamic potential $\Phi(\psi, \varphi)$ for the parameters $\alpha_{1\Gamma} < \alpha_{1X}$, $\alpha_{2\Gamma} > 0$, $\omega_\Gamma > 0$, $\beta_{1X} > 0$, and $W > 0$, where $\alpha^0_{1\Gamma} = \alpha_{1X}\alpha_{2\Gamma}/\mu_2$. The solid and dashed lines indicate the first-order and second-order phase transitions, respectively; and the thin solid line shows the thermodynamic path for sequence 1.

$$G_{3\Gamma} = \varphi_1^2\varphi_2^2\varphi_3^2, \quad G_{1X} = \sum_{i=1}^{3}\psi_i^2,$$

$$G_{2X} = \sum_{i=1}^{2}\sum_{j=2(i<j)}^{3}\psi_i^2\psi_j^2,$$

$$\Phi_{\Gamma X} = \mu_1\sum_{i=1}^{3}\varphi_i^2\psi_i^2$$

$$+ \mu_2[(\varphi_1^2 + \varphi_2^2)\psi_3^2 + (\varphi_2^2 + \varphi_3^2)\psi_1^2 + (\varphi_1^2 + \varphi_3^2)\psi_2^2].$$

Both the aforementioned reducible representations are critical; i.e., according to these representations, the system becomes unstable, and, hence, $\alpha_{1\Gamma} \longrightarrow 0$ and $\alpha_{1X} \longrightarrow 0$. In sequence 1, with a decrease in the temperature, first, the reducible representation φ and, then, the reducible representation ψ appear; therefore, we have $\alpha_{1\Gamma} < \alpha_{1X}$. In sequence 2, both the reducible representations appear simultaneously; therefore, we can set that $\alpha_{1\Gamma} \sim \alpha_{1X}$. The coefficients $\mu_i (i = 1, 2)$ characterize the interaction of the reducible representations φ and ψ. Upon the phase transition, the components of the new reducible representations are always orthogonal to each other; hence, we have $\mu_2 < \mu_1$. For definiteness, we assume that $\mu_2 < 0$ and $\mu_1 > 0$. Moreover, taking into account that the orderings are characterized by no more than one component of the reducible representation ψ, we can set that $\beta_{1X} > 0$.

Sequence 1 is formed as follows. Since $\alpha_{1\Gamma} < \alpha_{1X}$, under the conditions $\alpha_{1\Gamma} < 0$ and $\alpha_{1X} > 0$ there appears the reducible representation φ ($\psi = 0$). The diagrams of phase states described by the thermodynamic potential $\Phi_\Gamma$ are well known [20]. In the case where $\alpha_{2\Gamma} > 0$, $\omega_\Gamma > 0$, and $\sigma_\Gamma < 0$, the diagram of phase states has the form shown in Fig. 6 in the region $\alpha^0_{1\Gamma} < \alpha_{1\Gamma} \leq 0$. The phase (φ00) appears when $\alpha_{1\Gamma} < 0$ and $\beta_{1\Gamma} > 0$. As the temperature decreases, in the line $\beta_{1\Gamma} = -\sigma_\Gamma(-\alpha_{1\Gamma}/2\alpha_{2\Gamma})$ there occurs a first-order phase transition into the phase (φφ0). With a further decrease in the temperature, the coefficient $\alpha_{1X}$ decreases. At the coefficient $\alpha_{1X} = -2\mu_2(-\alpha_{1\Gamma}/2\alpha_{2\Gamma})$, the phase (φφ0) loses the stability with respect to the reducible representation ψ, and the phase (φφψ) is formed. The parameter determining the type of the phase transition into this phase can be written in the form $W = 4\alpha_{2\Gamma}\alpha_{2X} - \mu_2^2$. If $W > 0$, this transition is a second-order phase transition. If $W < 0$, this transition is a first-order phase transition. In the considered case, we have $W > 0$. The diagram of phase states described by the thermodynamic potential $\Phi(\psi, \varphi)$ is shown in Fig. 6.

For the formation of sequence 2, it is necessary that, first, the phase transition into the phase (φφψ) would become a first-order transition, and, second, the phase (φφψ) would have a common boundary with the symmetric cubic phase. The first of these requirements can be satisfied by making the parameter $W$ negative. In this case, the lines of the second-order phase transition between the phases (φφ0) and (φφψ) and also between the phases (φ00) and (φ0ψ) will turn into the lines of the first-order phase transition and become closer to the boundaries of the appearance of the reducible representation φ. Then, by decreasing the coefficient $\alpha_{1X}$ and making it closer to the coefficient $\alpha_{1\Gamma}$, we can obtain the phase (φφψ) at the boundary with the symmetric phase.

The parameter $\alpha_{1X}$ can be represented in the form $\alpha_{1X} = h + m\alpha_{1\Gamma}$ ($m \sim 1$), where $h$ is the value of $\alpha_{1X}$ when $\alpha_{1\Gamma} = 0$ ($h > 0$). The convergence of the coefficients $\alpha_{1X}$ and $\alpha_{1\Gamma}$ is due to the decrease in the value of $h$. A common boundary between the phase (φφψ) and the symmetric phase (000) arises under the conditions $h < (W + \alpha_{2X}\beta_{1\Gamma})^2/[-\mu_2 8\alpha_{2X}(2\alpha_{3\Gamma} + \delta_\Gamma)]$ and $W \lesssim 0$. In this case, the diagram of phase states will have the form shown in Fig. 7. The phase (φφψ) arises at the boundary with the symmetric phase, because the appearance of the reducible representation φ leads to a loss of the stability of the system with respect to the reducible representation ψ. As a result, there is a cocondensation of both the considered reducible representations, which leads to a trigger phase transition.

Thus, the diagram of phase states shown in Fig. 6 can be transformed into the diagram shown in Fig. 7 by changing the sign of the parameter $W$ from negative to positive and making the coefficients $\alpha_{1X}$ and $\alpha_{1\Gamma}$ closer to each other.

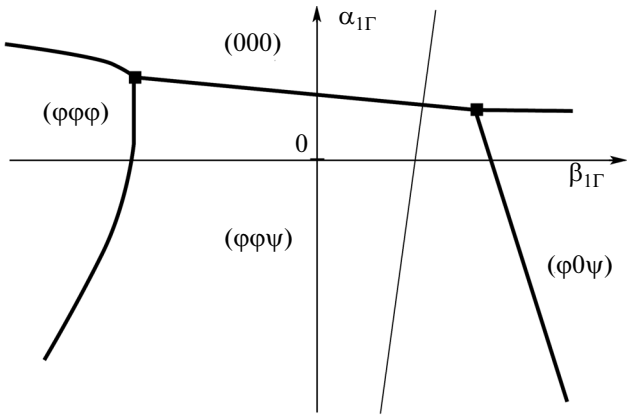


**Fig. 7.** Diagram of phase states described by the thermodynamic potential $\Phi(\psi, \varphi)$ for the parameters $\alpha_{1\Gamma} \sim \alpha_{1X}$, $\alpha_{2\Gamma} > 0$, $\omega_\Gamma > 0$, $\beta_{1X} > 0$, and $W < 0$. The solid line indicates the first-order phase transition, and the thin solid line shows the thermodynamic path for sequence 2.

## 4. DISCUSSION OF THE RESULTS

As was already noted, although the crystal-chemical parameters of the compounds under consideration are close to each other, the sets of their dissymmetric phases differ significantly. Since the subsystems of $B'F_6$ octahedra in these compounds are identical, it can be assumed that the aforementioned differences are associated in many aspects with the differences in the subsystems of alkali cations.

Among the factors, which play an important role in the formation of rotational instabilities, is the degree of correspondence between the sizes of particles in the crystal and the structure of the compound [1, 2]. In the simplest case, such degree of correspondence in elpasolite-type crystals is characterized by the packing coefficient $t$ [1, 2] (an analog of the tolerance factor), which has the form $t = (r_A + r_X)\sqrt{2}/(r_B + r_{B'} + 2r_X)$, where $r_A$, $r_B$, $r_{B'}$, and $r_X$ are the radii of $A$, $B$, $B'$, and $X$ ions, respectively.

For crystals $Rb_2KB'F_6$ ($B'$ = Ho, Dy, Tb) and $Cs_2RbDyF_6$, the packing coefficients are $t \approx 0.87$ and $\approx 0.89$, respectively. For packing coefficients $t < 1$, the $A$–$X$ bonds are stretched, while the $B$–$X$ and $B'$–$X$ bonds are compressed (see structural characteristics for $Cs_2RbDyF_6$ in [12] and for $Rb_2KHoF_6$ in Table 4). The subsystem of $BX_6$ and $B'X_6$ octahedra is subjected to compressive stresses, which contribute to the bending of the $B$–$X$–$B'$ bonds and favor the appearance of rotational distortions. Moreover, for $t < 1$, the sizes of the inter-octahedral (cuboctahedral) hole exceed the sizes of the $A$ cation. This creates favorable conditions both for octahedral rotations and for an increase in the root-mean-square deviations of the $A$ cations from the center of the hole, i.e., for an increase in the degree of its delocalization. The rotations corresponding to the $X_3^+$ mode induce a local field with the symmetry of the quadrupole moment in the inter-octahedral hole. The local field interacts with the $A$ cations, which have a "free space" in the hole. This decreases the energy of this mode and, hence, encourages its condensation. The interaction of the $\Gamma_4^+$ mode with the delocalized $A$ cations is substantially weaker, because, in the center of the hole, this mode induces a field with the symmetry of the third-order multipole moment. Consequently, with a further decrease in the packing coefficient $t$, an increase in the delocalization stimulates the "softness" of the system with respect to the $X_3^+$ mode to a greater extent than with respect to the $\Gamma_4^+$ mode.

## 5. CONCLUSIONS

The refined structures of the monoclinic phases of crystals $Rb_2KHoF_6$ (this work) and $Cs_2RbDyF_6$ [12] convincingly prove that critical distortions of the initial cubic elpasolite structure in these crystals are rotations of octahedral groups. However, in order to explain the available set of experimental data, it is necessary to take into account the noncritical displacements of atoms, which are reduced to octahedral distortions and displacements of Rb and Cs atoms located between the octahedra.

According to the structural data and phenomenological description, the evolution of phase states upon changing over from $Cs_2RbDyF_6$ to $Rb_2KB'F_6$ ($B'$ = Ho, Dy, Tb) can be represented as follows. For the packing coefficient $t \approx 0.89$ ($Cs_2RbDyF_6$), the sizes of the inter-octahedral hole significantly exceed the sizes of the $A$ cation. As a result, the crystal becomes unstable with respect to rotational distortions. This means that $\alpha_{1\Gamma} \longrightarrow 0$ and $\alpha_{1X} \longrightarrow 0$, but, since the reducible representation φ appears at 251 K and the reducible representation ψ appears at 196 K, we have $\alpha_{1\Gamma} < \alpha_{1X}$. With a further decrease in the packing coefficient $t$ ($t \approx 0.87$ for $Rb_2KHoF_6$), the parameters $\alpha_{1\Gamma}$ and $\alpha_{1X}$ decrease. This fact is confirmed by high values of isotropic thermal parameters $B_{iso}$ of Rb atoms in the cubic phase of the $Rb_2KHoF_6$ structure (Table 3) and those of Cs atoms in the cubic phase of the $Cs_2RbDyF_6$ structure [12]. However, the coefficient $\alpha_{1X}$ decreases more rapidly than the coefficient $\alpha_{1\Gamma}$. Consequently, the value of $\alpha_{1X}$ approaches the value of $\alpha_{1\Gamma}$. Simultaneously, since the indirect interaction of the reducible representations φ and ψ is enhanced through the displacements of the $A$ cations, which makes a negative contribution to $\mu_2$, this coefficient decreases (i.e., $|\mu_2|$ increases), and the parameter $W$ decreases and becomes negative. The enhancement of the indirect interaction in the phase (φφψ) is confirmed by the fact that, according to the obtained data, the displacement of Rb atoms from the center of the cuboctahedral hole

(~0.30 Å) in $Rb_2KHoF_6$ significantly exceeds the displacement of Cs atoms (~0.05 Å) in $Cs_2RbDyF_6$. Taken together, these changes lead to the fact that, in $Rb_2KB'F_6$ ($B'$ = Ho, Dy, Tb), the phase transition temperature increases and the phase ($\varphi\varphi\psi$) arises at the boundary with the symmetric phase.

Thus, the main factor determining the formation of phase states in these and related crystals is the mismatch in the crystal-chemical parameters of the components of the compounds and the elpasolite structure. As a result, the crystals are potentially unstable with respect to rotational distortion of two types. An important role in the formation of any rotational–distorted phase state is played by displacements of cations located in cuboctahedral holes.

## ACKNOWLEDGMENTS

This study was supported by the Ministry of Education and Science of the Russian Federation within the framework of the State Task for the Russian Siberian Federal University for Implementation of Scientific Research Work in 2014 (assignment no. 3.2534.2014/K).

## REFERENCES

1. K. S. Aleksandrov and B. V. Beznosikov, *Perovskite-Like Crystals* (Nauka, Novosibirsk, 1997) [in Russian].
2. K. S. Aleksandrov and B. V. Beznosikov, *Perovskites. Present and Future: Diversity of Paraphases, Phase Transformations, and Possibility of Synthesis of New Compounds* (Siberian Branch of the Russian Academy of Sciences, Novosibirsk, 2004) [in Russian].
3. S. V. Misyul', Sov. Phys. Crystallogr. **29** (5), 554 (1984).
4. K. S. Aleksandrov and S. V. Misyul', Sov. Phys. Crystallogr. **26** (5), 612 (1981).
5. K. S. Aleksandrov and J. Bartolome, Phase Transitions **74**, 255 (2001).
6. O. V. Kovalev, *Irreducible and Induced Representations and Co-Representations of Fedorov's Groups* (Nauka, Moscow, 1986) [in Russian].
7. S. C. Miller and W. F. Love, *Tables of Irreducible Representations of the Space Groups and Co-Representations of Magnetic Space Groups* (Pruett, Boulder, Colorado, United States, 1967).
8. V. P. Sakhnenko, V. M. Talanov, and G. M. Chechin, Fiz. Met. Metalloved. **62**, 847 (1986).
9. K. S. Aleksandrov, S. V. Misyul, and E. E. Baturinets, Ferroelectrics **354**, 60 (2007).
10. M. V. Gorev, I. M. Iskornev, L. A. Kot, S. V. Misyul', and I. N. Flerov, Sov. Phys. Solid State **27** (6), 1035 (1985).
11. K. S. Aleksandrov, S. V. Melnikova, and S. V. Misjul, Phys. Status Solidi A **104**, 545 (1987).
12. S. V. Misyul', M. S. Molokeev, L. V. Osokina, and I. N. Safonov, J. Sib. Fed. Univ.: Math. Phys. **5** (4), 566 (2012).
13. V. N. Voronov, M. V. Gorev, S. V. Mel'nikova, S. V. Misyul', and I. N. Flerov, Sov. Phys. Solid State **33** (10), 1663 (1991).
14. M. V. Gorev, I. N. Flerov, V. N. Voronov, and S. V. Misyul', Phys. Solid State **35** (4), 524 (1993).
15. *Bruker AXS: TOPAS V4. General Profile and Structure Analysis Software for Powder Diffraction Data. User's Manual* (Bruker AXS, Karlsruhe, Germany, 2008).
16. B. J. Campbell, H. T. Stokes, D. E. Tanner, and D. M. Hatch, J. Appl. Crystallogr. **39**, 607 (2006).
17. L. D. Landau and E. M. Lifshitz, *Course of Theoretical Physics*, Vol. 5: *Statistical Physics, Part 1* (Nauka, Moscow, 1973; Butterworth–Heinemann, Oxford, 1980).
18. M. P. Ivliev, Crystallogr. Rep. **47** (6), 996 (2002).
19. M. P. Ivliev, I. P. Raevskii, S. I. Raevskaya, V. A. Shuvaeva, and I. N. Pirog, Phys. Solid State **49** (4), 769 (2007).
20. Yu. M. Gufan, *Structural Phase Transitions* (Nauka, Moscow, 1982) [in Russian].

*Translated by O. Borovik-Romanova*